Optimization of Monte Carlo calculations of the effective potential

A. Ardekani* and A. G. Williams†
Department of Physics and Mathematical Physics and Special Research Center for the Subatomic Structure of Matter, University of Adelaide, Adelaide, SA 5005, Australia
(Received 21 May 1997)

We study Monte Carlo calculations of the effective potential for a scalar field theory using three techniques. In each case we extract the renormalized quantities of the theory. The system studied in our calculations is a one-component ϕ^4 model in two dimensions. We apply these methods to both the weak and strong coupling regimes. In the weak coupling regime we compare our results for the renormalized quantities with those obtained from two-loop lattice perturbation theory. Our results are verified in the strong coupling regime through comparison with the strong coupling expansion. We conclude that effective potential methods, when suitably chosen, can be accurate tools in calculations of the renormalized parameters of scalar field theories. [S1063-651X(98)09801-8]

PACS number(s): 02.70.−c, 11.10.Kk, 11.15.Ha, 11.15.Tk

I. INTRODUCTION

An understanding of the underlying vacuum structure of a quantum field theory is essential for understanding its physical content. This analysis is conveniently carried out by calculating a quantity known as the effective potential [1–3], denoted by $U(\bar{\phi})$ and the minimum of which gives information as to the nature of the lowest energy eigenstate of the theory. This makes $U(\bar{\phi})$ very useful, particularly in studies of spontaneous symmetry breaking (SSB). The effective potential determines the one-particle irreducible (1PI) vertices [1] at zero momenta and reflects any nontrivial dynamics. It is also widely used to study radiative corrections in quantum field theories [3]. Truncating the loop expansion of the effective potential often gives it a complex and nonconvex character, in spite of the fact that on general grounds the effective potential must be real and of convex character [4]. It has been pointed out that the loop expansion for the effective potential fails for the fields in just those regions where the classical potential is nonconvex; the most familiar case corresponds to a double-well potential [5]. Therefore it is important to carry out nonperturbative studies which can be used even where the loop expansion is not applicable. One convenient nonperturbative approach is to employ a discrete version of the theory, i.e., lattice field theory. Lattice field theories have an ultraviolet (UV) regulator (the lattice spacing) and an infrared (IR) cutoff (the lattice size) and are conveniently studied using Monte Carlo (MC) methods.

The model used in our study is the $\lambda\phi^4_{1+1}$ model. The Higgs mechanism is based on a more elaborate version of such a model and is usually discussed at the tree level. A fully nonperturbative treatment of the Higgs model would be of considerable interest, but is not discussed further here. First, we review the lattice effective potential, showing how all of the renormalized vertex functions can be calculated if one knows the full structure of the effective potential. Then, we investigate the calculation of the effective potential for $\lambda\phi^4$ using two established methods: The variation of source method (VSM) [6,7] which introduces an external field such that the effective potential can be calculated from the response of the system to this external field; and a version of the constraint effective potential (CEP I) [8] where the effective potential is calculated from the distribution of the constrained mean field, $\bar{\phi}$. Some suggestions for improving these methods are also put to the test. We will show that the standard method of calculating the renormalized coupling in $\lambda\phi^4$ theory, through calculating two- and four-point correlation functions at zero momentum, suffers from large statistical errors, especially where the coupling constant is not sufficiently strong. CEP I also suffers from the same problem. We will show that the VSM can be used to obtain much more accurate and precise results for the renormalized vertex functions. In addition to the above two established methods using the effective potential (VSM and CEP I) we will show how the renormalized quantities can be calculated from the effective potential by calculating appropriate correlation functions in the presence of a constraint, $\bar{\phi}$ (we refer to this method as CEP II). The procedure does not require any curve fitting or extrapolation to a zero external field limit, as VSM requires. Also this method does not require the very high statistics that the CEP I method needs. The computational time is also dramatically reduced. However, the drawback is that its accuracy in the strong coupling regime is limited. We will point out the advantages and disadvantages of each method and their accuracy.

Both in numerical MC studies and analytical calculations it is important to find the renormalization group trajectories (RGT). Along these curves and close to an infrared fixed point (the scaling region) the physics described by the lattice regularized quantum field is invariant and only the value of the cutoff (lattice spacing) is changing. It is in the scaling region that the ratio of dimensionless renormalized vertex functions is invariant and one expects the scaling region to be in the vicinity of the critical point. However, we perform our calculations away from the scaling region in order to examine the accuracy of effective potential methods to the

*Electronic address: aardekan@physics.adelaide.edu.au
†Electronic address: awilliam@physics.adelaide.edu.au

fullest extent. Since the correlation length is large in the scaling region, one expects that the finite size effects can be considerable. By performing the calculations in a region away from the scaling region, where the correlation length is smaller, we have hopefully minimized the finite size effects on our calculations of renormalized quantities. The other factor is that away from the critical point Monte Carlo methods typically perform well, whereas, near the critical point where the correlation length becomes larger, the autocorrelation length rapidly diverges. This well-known phenomenon results in critical slowing down and causes some well-known complications. Hence, we prefer here to perform our calculations away from the critical point. In the weak coupling regime we compare our results with lattice perturbation theory results in order to establish the absence of finite size effects in our calculations. In the strong coupling regime we compare the effective potential results with the results obtained from the strong coupling expansion on the lattice, extrapolated to a larger correlation length. The effective potential methods discussed here can be accurate tools for finding the scaling region, since they can provide accurate values for the dimensionless ratios of renormalized parameters as will become evident. In the case of $\lambda\phi^4$ the fixed points can be calculated perturbatively [10]. Nonperturbatively, the parameter points on the second-order phase transition critical line which separates the two phases, $\langle\phi\rangle=0$ and $\langle\phi\rangle\neq 0$, are good candidates for the IR fixed points (the point $\hat{m}^2=\hat{\lambda}=0$ is the trivial fixed point and any scaling region corresponding to this fixed point represents a free field theory).

In Sec. II we briefly summarize the model to be studied. In Sec. III we review the above methods of calculation of the effective potential. In Sec. IV we perform the calculations for both the symmetric and the spontaneous symmetry breaking cases in the weak coupling regime and we compare our results with those obtained from lattice perturbation theory. We also perform calculations in the strong coupling regime and compare these with the strong coupling expansion.

II. THE $\lambda\phi^4$ MODEL

We start with the action of a single component $\lambda\phi^4$ theory in d dimensions in Euclidean space in the presence of a source J (in units where $\hbar=c=1$),

$$S[\phi,J]=\int d^dx\,\frac{1}{2}(\partial_\mu\phi)^2+\frac{1}{2}m^2\phi^2+\frac{\lambda}{4!}\phi^4-J\phi.$$

A discrete lattice version of the action can be written as

$$S[\hat{\phi},\hat{J}]=\left[\frac{1}{2}\sum_{n,\mu}(\hat{\phi}_{n,\mu}-\hat{\phi}_n)^2+\frac{1}{2}\sum_n\hat{m}^2\hat{\phi}_n^2+\sum_n\frac{\hat{\lambda}}{4!}\hat{\phi}_n^4-\sum_n\hat{J}_n\hat{\phi}_n\right], \tag{1}$$

where we have defined the dimensionless quantities $\hat{\phi}\equiv a^{(d/2)-1}\phi$, $\hat{m}\equiv ma$, and $\hat{\lambda}\equiv\lambda a^{4-d}$ and $\hat{J}\equiv a^{(d/2)+1}J$. In addition $n\equiv(n_1,\ldots,n_d)$ is a d-dimensional vector labeling the lattice sites and μ is a unit vector in the temporal or spatial direction. The sum over μ is over the d Euclidean directions. We also have denoted the field on the neighboring site of n in the direction of μ by $\hat{\phi}_{n,\mu}$. Henceforth we drop the hat from the dimensionless field variables and sources for brevity unless it is necessary to avoid confusion. We also impose the appropriate periodic boundary condition on fields:

$$\phi_{n+\hat{N}_\mu}=\phi_n \quad \text{for all } \mu, \tag{2}$$

where $\hat{N}_\mu=(0,\ldots,N_\mu,\ldots,0)$, is a d-dimensional vector with N_μ being the number of lattice sites in the direction μ.

The ϕ^4 theory is known to exist in two phases, one where the reflection symmetry $\phi\rightarrow-\phi$ is spontaneously broken and the other where it is not. The symmetric phase with $\langle\phi\rangle=0$ is separated from the broken symmetry phase with $\langle\phi\rangle\neq 0$ by a line of second-order phase transitions where $\hat{m}$ and $\hat{\lambda}$ assume the critical values $\hat{m}_c$ and $\hat{\lambda}_c$.

For the action $S[\phi]$ on the lattice the generating functional for the correlation functions is defined as

$$Z[J]=\frac{\int[d\phi]e^{-S[\phi,J]}}{\int[d\phi]e^{-S[\phi]}}, \tag{3}$$

such that $Z[0]=1$. From $Z[J]$ one can define the connected Green functions as

$$G(n_1,\ldots,n_j)_c=\frac{\partial}{\partial J_{n_1}}\cdots\frac{\partial}{\partial J_{n_j}}W[J]\big|_{J=0}, \tag{4}$$

where

$$W[J]=\ln Z[J]. \tag{5}$$

III. THE LATTICE EFFECTIVE POTENTIAL

Consider a lattice Lagrangian density on a d-dimensional cubic lattice with the total number of lattice sites N^d,

$$\mathcal{L}_n=\sum_\mu\frac{1}{2}(\phi_{n,\mu}-\phi_n)^2+V(\phi_n). \tag{6}$$

The classical vacuum (ground state) is at the minimum of $V(\phi)$. The vacuum expectation value $\langle\phi\rangle$ of the quantum field is not necessarily identical to the classical vacuum. The vacuum expectation value of the field in the presence of an external source, $J(x)$, is given by

$$\phi_{cn}[J]\equiv\frac{\partial W[J]}{\partial J_n}. \tag{7}$$

The vacuum expectation value $\langle\phi\rangle$ is the limit of ϕ_{cn} as $J\rightarrow 0$. Hence we can ask for what value of J can one obtain a given ϕ_c. One can choose to treat ϕ_c as the independent variable instead of J and define the ''effective action'' $\Gamma[\phi_c]$ by a Legendre transformation:

$$\Gamma[\phi_c]=\sum_n\phi_{cn}J_n-W[J], \tag{8}$$

where ϕ_c is defined in Eq. (7). It is easy to verify that

$$J_n[\phi_c] \equiv \frac{\partial \Gamma[\phi_c]}{\partial \phi_{cn}}. \tag{9}$$

In the case $J=0$, by translational invariance it follows that ϕ_c must become constant (i.e., independent of the label n). Hence the vacuum expectation value is given by $\langle\phi\rangle$ and satisfies

$$\left.\frac{d\Gamma[\phi_c]}{d\phi_c}\right|_{\phi_c=\langle\phi\rangle} = 0. \tag{10}$$

Similarly for any constant J we must have $\phi_c=\overline{\phi}$ also constant. Define the effective potential $U(\overline{\phi})$ by

$$\Gamma[\overline{\phi}] = N^d U(\overline{\phi}). \tag{11}$$

The Fourier trasform on a finite, discrete lattice is defined by

$$\widetilde{\phi}_k \equiv \sum_n e^{2\pi i n.\hat{k}/N}\phi_n, \tag{12}$$

where $\hat{k}\equiv\hat{k}_1,\ldots,\hat{k}_d$ is a d-dimensional vector with $(-N/2)<\hat{k}_n\leq N/2$ (we assume N is even from this point) and where $n\cdot\hat{k}\equiv n_1\hat{k}_1+\cdots+n_d\hat{k}_d$. The coordinate-space and momentum-space δ functions are

$$\delta_{m,n}=\frac{1}{N^d}\sum_{\hat{k}} e^{-2\pi i(n-m)\hat{k}/N}, \quad \delta_{\hat{k},\hat{q}}=\frac{1}{N^d}\sum_n e^{-2\pi i(\hat{k}-\hat{q})n/N}, \tag{13}$$

respectively. The inverse Fourier transform is

$$\phi_n=\frac{1}{N^d}\sum_{\hat{k}} e^{-2\pi i n\hat{k}/N}\widetilde{\phi}_{\hat{k}}.$$

Note that we have used the asymmetric normalization of the Fourier transform and its inverse as is usual in the field theory in the continuum. The effective action is the generator of proper (i.e., one-particle irreducible) Green's functions and in particular we can Taylor expand the effective action to give

$$\Gamma[\phi_c]=\sum_{M=0}^{\infty}\frac{1}{M!}\sum_{n_1,\ldots,n_M}\Gamma^{(M)}(n_1,\ldots,n_M)\phi_{cn_1}\cdots\phi_{cn_M}. \tag{14}$$

Here $\Gamma^{(M)}(n_1,\ldots,n_M)$ are the proper M-point Green functions in the presence of the source J_n,

$$\frac{\partial^M\Gamma[\phi]}{\partial\phi_{cn_1}\cdots\partial\phi_{cn_M}}=\Gamma^{(M)}(n_1,\ldots,n_M). \tag{15}$$

In terms of its Fourier transforms we have

$$\Gamma[\phi_c]=\sum_{M=0}^{\infty}\frac{1}{M!}\frac{1}{N^{Md}}\sum_{\hat{k}_1,\ldots,\hat{k}_M} \times\widetilde{\Gamma}^{(M)}(\hat{k}_1,\ldots,\hat{k}_M)\widetilde{\phi}_{-\hat{k}_1}\cdots\widetilde{\phi}_{-\hat{k}_M}, \tag{16}$$

where here $\widetilde{\phi}$ is the Fourier transform of ϕ_c.

The vacuum proper Green functions are obtained by setting $J=0$. If the source is a constant ($J_n=J$ for all n), then the translational invariance is restored and we can factor out an overall normalization and a δ function to define

$$\widetilde{\Gamma}^{(M)}(\hat{k}_1,\ldots,\hat{k}_M)\equiv N^d\delta_{0,\hat{k}_1+\cdots+\hat{k}_M}\widetilde{\Gamma}_c^{(M)}(\hat{k}_1,\ldots,\hat{k}_M), \tag{17}$$

where in the limit $J\to 0$ we recognize that $\widetilde{\Gamma}_c^{(M)}(\hat{k}_1,\ldots,\hat{k}_M)$ is the dimensionless, lattice equivalent of the proper M-point Green function in momentum space. For constant J we also have $\phi_{cn}\to\overline{\phi}$ and hence $\widetilde{\phi}=N^d\delta_{\hat{k},0}\overline{\phi}$ and Eq. (16) gives

$$\Gamma(\overline{\phi})=N^d\sum_{M=0}\frac{1}{M!}\widetilde{\Gamma}_c^{(M)}(0)\overline{\phi}^M, \tag{18}$$

where

$$\widetilde{\Gamma}_c^{(M)}(0)\equiv\widetilde{\Gamma}_c^{(M)}(0,\ldots,0). \tag{19}$$

Comparing Eq. (11) with Eq. (16) gives

$$U(\overline{\phi})=\sum_{M=0}^{\infty}\frac{1}{M!}\widetilde{\Gamma}_c^{(M)}(0)\overline{\phi}^M. \tag{20}$$

It immediately follows that

$$\left.\frac{d^M U(\overline{\phi})}{d\overline{\phi}^M}\right|_{\overline{\phi}=\langle\phi\rangle=0}=\widetilde{\Gamma}_c^{(M)}(0), \tag{21}$$

where here it is understood that we are working in the unbroken symmetry sector, $\langle\phi\rangle=0$. In the unbroken sector we see from Eq. (20) that the dimensionless, proper Green functions with vanishing momenta can be easily obtained from the effective potential $U(\phi)$ by differentiation. We see that $\overline{\phi}$ minimizes $U(\overline{\phi})$ and in the limit $J\to 0$ the minimum $\overline{\phi}\to\langle\phi\rangle$. Also note that Eq. (9) gives an expansion of J in terms of the $\overline{\phi}$'s and $\Gamma(0)$'s,

$$J(\overline{\phi})=N^d\sum_{M=1}^{\infty}\frac{1}{(M-1)!}\widetilde{\Gamma}_c^{(M)}(0)\overline{\phi}^{M-1}. \tag{22}$$

In the broken symmetry sector, $\langle\phi\rangle\neq 0$, it is more appropriate to use the shifted field

$$\chi(x)\equiv\phi(x)-\langle\phi\rangle. \tag{23}$$

The one-particle irreducible vertex functions $\Gamma_{(s)}^{(M)}$ are linear combination of the $\Gamma^{(M)}$'s, and can be obtained from the shifted version of Eq. (20),

$$U(\overline{\phi})\equiv U_{(s)}(\overline{\chi})=U_{(s)}(\overline{\phi}-\langle\phi\rangle) =\sum_{M=0}^{\infty}\frac{[\overline{\phi}-\langle\phi\rangle]^M}{M!}\widetilde{\Gamma}_{(s)}^{(M)}(0). \tag{24}$$

As is usually done in lattice field theory studies we renormalize at the renormalization point where all external momenta of the Green functions vanish. The renormalized

quantities can be obtained directly from the effective potential. For example, in the $\lambda\phi^4$ theory we have

$$\left.\frac{dU(\bar{\phi})}{d\bar{\phi}}\right|_{\bar{\phi}=\langle\phi\rangle}=0, \tag{25}$$

$$Z\left.\frac{d^2U(\bar{\phi})}{d^2\bar{\phi}}\right|_{\bar{\phi}=\langle\phi\rangle}=Z\tilde{\Gamma}_c^{(2)}(0)=\tilde{\Gamma}_r^{(2)}=\hat{m}_r^2, \tag{26}$$

$$Z^2\left.\frac{d^4U(\bar{\phi})}{d^4\bar{\phi}}\right|_{\bar{\phi}=\langle\phi\rangle}=Z^2\tilde{\Gamma}_c^{(4)}(0)=\tilde{\Gamma}_r^{(4)}=\hat{\lambda}_r, \tag{27}$$

where Z is the field wave function renormalization constant ($\phi_r=\sqrt{Z}\phi$). From the first two conditions above and requiring $\hat{m}_r^2\geqslant 0$ it follows that $\langle\phi\rangle$ is at the minimum of $U(\bar{\phi})$. Also note that $\hat{m}_r$ and $\hat{\lambda}_r$ defined as above are not the physical mass and coupling, which are defined in the pole of the propagator in the complex energy plane and the on shell four-point function, respectively. However, in the scaling region (close to the critical line) these values are a good approximation to the physical mass and coupling [9].

IV. THE MC EFFECTIVE POTENTIAL

In this section we will examine three MC methods for calculation of the lattice effective potential. The renomalized coupling constants obtained by these methods are compared with analytical results. From this point on we work exclusively in two dimensions ($d=2$).

A. The variation of source method

Equation (22) suggests that in the Monte Carlo calculation one can calculate the mean value of the fields, $\bar{\phi}$, for different values of the source and as a result one obtains $\bar{\phi}$ as a function of J. This function can then be inverted to obtain J as a function of $\bar{\phi}$, i.e., $J(\bar{\phi})$. Then using Eq. (22) we see that the derivatives of J with respect to $\bar{\phi}$ would give the proper Green functions at zero momentum. From Eq. (7) one also concludes that $\bar{\phi}_J$ is antisymmetric in J. That is,

$$\bar{\phi}_J=-\bar{\phi}_{-J}. \tag{28}$$

Figure 1 shows $J(\bar{\phi})$ as a function of $\bar{\phi}$ for the symmetric case [Fig. 1(a)] and the broken symmetry case [Fig. 1(b)]. Note that for the broken symmetry case, $\bar{\phi}_J$ as a function of J is discontinuous and so the relation in Eq. (22) cannot be inverted for all $\bar{\phi}(J)$. Whenever it is possible Eq. (22) has to be inverted to obtain the source J as a function of $\bar{\phi}$. Then the derivatives of J with respect to $\bar{\phi}$ would give the vertex functions at zero momenta and consequently the renormalized masses and couplings can be calculated.

The mean value of the field in the presence of a source has a small statistical error. This is expected since it is an analog to the reduction of fluctuations of a spin system in the presence of an external magnetic field. As the source becomes smaller the fluctuations become larger. Thus one needs to perform the calculations for large enough sources that the error is small and then extrapolate the results to $J=0$.

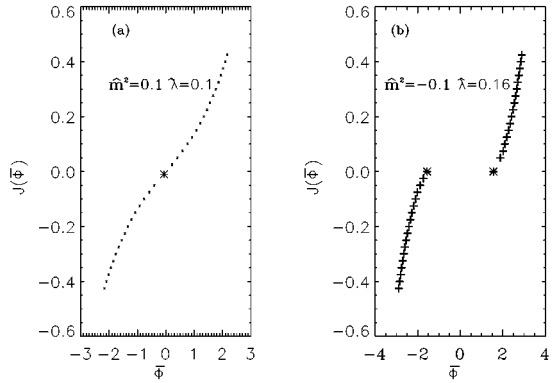

FIG. 1. Examples of $J(\bar{\phi})$ versus $\bar{\phi}$ in the symmetric sector (a) and for the broken symmetry sector (b). The stars (*) correspond to the values of $\bar{\phi}$ at $J=0$. For these results $N=20$.

This method will be referred to as the variation of source method and has a number of advantages. The vacuum expectation values of the field $\bar{\phi}(J)$ are the simplest quantities to compute on the lattice and their J dependence can be exploited to get the first derivative of the effective potential. Since the source effectively causes the boson field to become more massive, the finite size effects generated by the lattice become exponentially small provided that the lattice is large enough. Since the data become noisy for small values of J we need to restrict the analysis to a safe region of J, which can introduce some errors in the results through uncertainties in the extrapolation.

B. The constraint effective potential (CEP I)

In the preceding section the effective action and the effective potential $U(\bar{\phi})$ were defined through the introduction of a source J. There is a different method which does not require such a dynamical symmetry breaking source. The constraint effective potential was introduced by Fukuta and Kyrikopoulos [8] as an alternative way of obtaining the explicit expression for the effective potential. It was further analyzed by O'Raifeartaigh, Wipf, and Yoneyama [11]. In this approach one obtains an explicit expression for the effective potential, without introducing external sources, but instead through the introduction of a δ function in the functional integral. In the constraint effective potential approach one first defines $\tilde{U}(\bar{\phi})\equiv U(N^2,\bar{\phi})$ as

$$e^{-N^2\tilde{U}(\bar{\phi})}=\int[d\phi]\delta\left(\frac{1}{N^2}\sum_n\phi_n-\bar{\phi}\right)e^{-S[\phi]} \tag{29}$$

and then uses the fact that as $N^2\to\infty$ we have $\tilde{U}(\bar{\phi})\to U(\bar{\phi})$ and the effective potential is recovered.

It is easiest to demonstrate this result in Minkowski space, where Eq. (29) becomes

$$e^{-iN^2\tilde{U}(\bar{\phi})}=\int[d\phi]\delta\left(\frac{1}{N^2}\sum_n\phi_n-\bar{\phi}\right)e^{iS[\phi]}. \tag{30}$$

We can replace the δ function in Eq. (30) by its integral representation to obtain (up to an irrelevant constant)

$$e^{-iN^2\tilde{U}(\bar{\phi})} = C\int dJ \int [d\phi] e^{i\int dx[\mathcal{L}+J\phi]-iN^2\bar{\phi}J}$$

$$= C'\int dJ e^{i(W[J]-N^2J\bar{\phi})}. \tag{31}$$

Note that in the integrand of Eq. (31) we have $\bar{\phi}$ fixed and J arbitrary. In the limit $N^2\to\infty$ the dominate contribution to the integral comes from the stationary point of the integral which is the value of J at which $dW[J]/dJ=\bar{\phi}$. Recall that $\Gamma(\bar{\phi})=(J\bar{\phi}-W[J])|_{\bar{\phi}=dW[J]/dJ}$, from which we see that up to an irrelevant overall constant

$$e^{-iN^2\tilde{U}(\bar{\phi})}\to e^{-i\Gamma(\bar{\phi})}=e^{-iN^2U(\bar{\phi})} \quad \text{as} \quad N^2\to\infty, \tag{32}$$

as claimed.

We can also arrive at this result directly in Euclidean space by multiplying both sides of Eq. (29) by $e^{N^2J\bar{\phi}}$ with J arbitrary and then integrating over $\bar{\phi}$ to obtain

$$\int d\bar{\phi} e^{-N^2[\tilde{U}(\bar{\phi})-J\bar{\phi}]} = \int [d\phi] e^{-S[\phi]+J\Sigma_n\phi_n}. \tag{33}$$

As $N^2\to\infty$ the left hand side of Eq. (33) becomes entirely dominated by the stationary point of the one-dimensional $\bar{\phi}$ integration given by $d\tilde{U}(\bar{\phi})/d\bar{\phi}=J$, while the right hand side is recognized as $e^{W[J]}$ for a constant source, J. Hence up to an irrelevant overall constant we find

$$e^{-N^2[\tilde{U}(\bar{\phi})-J\bar{\phi}]}\to e^{W[J]} \quad \text{as} \quad N^2\to\infty, \tag{34}$$

and so find that (up to a constant)

$$e^{-N^2\tilde{U}(\bar{\phi})}\to e^{W[J]-N^2J\bar{\phi}}=e^{-N^2U(\bar{\phi})} \quad \text{as} \quad N^2\to\infty, \tag{35}$$

as required.

It is important to note that the $e^{-N^2\tilde{U}(\bar{\phi})}$ relates to similar definitions in statistical mechanics and spin systems [12] and that

$$P(\bar{\phi})=\frac{e^{-N^2\tilde{U}(\bar{\phi})}}{\int d\bar{\phi} e^{-N^2\tilde{U}(\bar{\phi})}} \tag{36}$$

can be interpreted as the probability density for the system to be in a state of ''magnetization,'' $\bar{\phi}$. Then it can be seen that the probability for a state whose average field is not a minimum of $\tilde{U}(\bar{\phi})$ then decreases as $N^2\to\infty$.

This suggests that one needs to study the probability distribution of the order parameter $\bar{\phi}$. Using a Monte Carlo algorithm one generates a Boltzmann ensemble of configurations, $\{\phi\}$, weighted by $e^{-S[\phi]}$. Let $d\mathcal{N}$ be the number of configurations with average field values in an interval $d\bar{\phi}$ about $\bar{\phi}$. Then

$$d\mathcal{N}(\bar{\phi})=Ce^{-N^2\tilde{U}(\bar{\phi})}d\bar{\phi}, \tag{37}$$

with C some constant. Then one can write

$$\tilde{U}(\bar{\phi})=-\frac{1}{N^2}\ln\frac{d\mathcal{N}(\bar{\phi})}{d\bar{\phi}}, \tag{38}$$

up to an irrelevant additive constant. Equation (36) suggests that one can generate a large number of configurations weighted by $e^{-S[\phi]}$, calculate $\bar{\phi}$ for each configuration, and construct a normalized histogram. The histogram can be fitted to Eq. (38). The most probable average field values are near the minimum of the effective potential. In order to determine $\tilde{U}(\bar{\phi})$ away from its minimum, i.e., to sample a range of relatively improbable values of $\bar{\phi}$, one can introduce a small source. Then a simple generalization of Eq. (36) allows a nonzero external source [13]

$$\tilde{U}(\bar{\phi})-J\bar{\phi}=-\frac{1}{N^2}\ln\frac{d\mathcal{N}(\bar{\phi})}{d\bar{\phi}}. \tag{39}$$

Thus one can check whether such an ansatz gives a good approximation for the effective potential, and so construct the effective potential by performing a simultaneous fit of several histograms corresponding to different values of J. By the expression ''simultaneous fit,'' we mean that the χ^2 values corresponding to each J are summed and this sum is then minimized. This method can be applied easily on the lattice. Note that in Eq. (36) we have assumed that for sufficiently large N^2 the finite volume effects on $\tilde{U}(\bar{\phi})$ can be neglected, i.e., that the lattice volume is sufficiently large. The constraint effective potential method summarized in Eq. (39) will be referred to as CEP I.

C. The constraint effective potential (CEP II)

Now return to Eq. (29) and perform a shift of field, $\phi(x)\to\phi(x)+\bar{\phi}$. Since the measure is translationally invariant we obtain

$$e^{-N^2\tilde{U}(\bar{\phi})}=\int [d\phi]\delta\left(\frac{1}{N^2}\sum_n \phi_n\right)e^{-S[\phi+\bar{\phi}]}. \tag{40}$$

Taking the derivative with respect to $\bar{\phi}$ we get

$$\frac{d\tilde{U}(\bar{\phi})}{d\bar{\phi}}e^{-N^2\tilde{U}(\bar{\phi})}=\frac{1}{N^2}\int [d\phi]\delta\left(\frac{\Sigma\phi_n}{N^2}\right)$$

$$\times\frac{dS(\phi+\bar{\phi})}{d\bar{\phi}}e^{-S[\phi+\bar{\phi}]}. \tag{41}$$

Only the potential part of the action is affected by the shift of field since $\bar{\phi}$ is constant and so $dS/d\bar{\phi}=N^2dV/d\bar{\phi}$. Using this fact and shifting the field back to its original form then gives

$$\frac{d\tilde{U}(\bar{\phi})}{d\bar{\phi}}=\left\langle\frac{dV(\phi)}{d\phi}\right\rangle_{\bar{\phi}}, \tag{42}$$

where we have introduced the shorthand notation

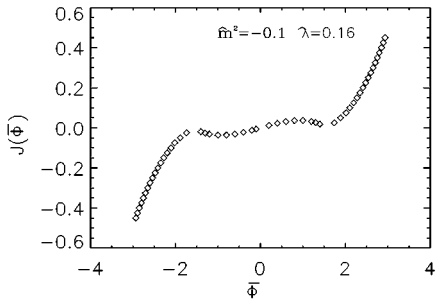

FIG. 2. An example of $J(\bar{\phi})$ versus $\bar{\phi}$ in the broken sector using the constraint effective potential. For these results $N=20$.

$$\langle O(\phi)\rangle_{\bar{\phi}} \equiv (e^{N^2\tilde{U}(\bar{\phi})}) \int [d\phi]\delta\left(\frac{1}{N^2}\sum_n \phi_n - \bar{\phi}\right) \times O(\phi)e^{-S[\phi]}. \tag{43}$$

In the $\lambda\phi^4$ theory being considered here we find

$$\frac{d\tilde{U}(\bar{\phi})}{d\bar{\phi}} = \hat{m}^2\bar{\phi} + \frac{\hat{\lambda}}{6}\langle\phi^3\rangle_{\bar{\phi}}. \tag{44}$$

Expressions for some of the higher derivatives of $U(\bar{\phi})$ are given in the Appendix. These equations are very useful in the Monte Carlo calculations since they relate the derivatives of the effective potential (and consequently the zero momentum vertex function) to the averages of quantities that can be calculated directly from the lattice. This method will be referred to as CEP II.

There are two ways of calculating the renormalized quantities using CEP II. The first one applies the constraint on the lattice, fixing $\bar{\phi}$, then calculates $\langle\phi^3\rangle$, and finally uses Eq. (44) to obtain the first derivative of the effective potential. Higher derivatives are evaluated from fitting a curve to the $d\tilde{U}/d\bar{\phi}$ versus $\bar{\phi}$ results. This has some similarities to the variation of source method; however, there is a difference between these two methods. In VSM one sets the source J to constant and $\langle\phi\rangle=\bar{\phi}$ up to fluctuations due to finite N^2, whereas in CEP II we have $\langle\phi\rangle=\bar{\phi}$ exactly by construction.

In the broken symmetry sector there is another difference between this method and VSM in the broken sector. When using VSM we are not able to obtain any value of $\langle\phi\rangle$ in the region between the two minima, whereas both CEP methods are suitable for probing this region. One can always fix $\bar{\phi}$ to any value including the values between the two minima to get the full shape of $J(\bar{\phi})$ (see Fig. 2). However, as far as the practical calculation of renormalized quantities is concerned, this method is almost equivalent to VSM and so from here on we disregard this approach.

The second approach to CEP II is through the equations shown in the Appendix and is more direct. These equations relate the derivative of the effective potential to the averages of some derivatives of the classical potential. All these averages should be taken in the presence of the constraint which fixes $\langle\phi\rangle=\bar{\phi}$.

We imposed the constraint using hybrid Monte Carlo. The constraint can be taken into account by appropriately adjusting an arbitrarily chosen single site variable ϕ_k. Consider an initial configuration (denoted C) with the field average being $\bar{\phi}$. Each time a site is updated by a value δ, that is,

$$\phi_i' = \phi_i + \delta,$$

then the chosen site ϕ_k must be updated simultaneously by $\phi_k' = \phi_k - \delta$. This procedure is carried out for all the sites, which completes a sweep; the next sweep then starts again from ϕ_1. In order to have a Markov chain which converges to the equilibrium state, one requires that the process be ergodic and that the detailed balance condition be satisfied (i.e., the detailed balance condition is a sufficient but not a necessary condition to converge to the equilibrium state). In the hybrid Monte Carlo algorithm ergodicity is built into the algorithm by performing Langevin updating for some number of times (say N''). Here we chose N'' to be 3. The detailed balance condition is satisfied through a Metropolis test. That is, after a complete sweep the new configuration (denoted C') is accepted with probability

$$p = \min\{1, e^{-H[C']}/e^{-H[C]}\},$$

where H is the hybrid Monte Carlo Hamiltonian. It is not difficult to see that, in general, imposing the constraint does not prevent us from constructing a suitable Markov chain.

The advantage of this method over the VSM is that one does not need to run a Monte Carlo routine several times with different sources, and no curve fitting is required. One disadvantage of this method is that for calculation of the renormalized coupling one needs to add and subtract many average terms as has been shown in the Appendix. Although the statistical errors might be small for each term, the overall errors contributing to the renormalized coupling can be large. However, the renormalized mass in the symmetric phase of the $\lambda\phi^4$ theory obtained using this method is very accurate.

We also would like to comment on Fig. 2. It has been shown by a very general argument that $U''(\bar{\phi}) \geqslant 0$ for all $\bar{\phi}$ [4] (primes denote differentiation with respect to $\bar{\phi}$). This general property is known as the ‘‘ convexity’’ of the effective potential. Looking at Fig. 2 it is clear that this condition is violated for $\tilde{U}(\bar{\phi})$. This can be understood by noting that convexity holds only in the thermodynamical limit, i.e., $N^2 \rightarrow \infty$.

To conclude this section it should also be mentioned that the proper vertex functions can be obtained directly using the standard Monte Carlo method. For example, for the $\lambda\phi^4$ four-point vertex function one obtains

$$\tilde{\Gamma}_c^{(4)}(0) = -\frac{\langle\tilde{\phi}^4\rangle_c - 3\langle\tilde{\phi}^2\rangle_c^2}{\langle\tilde{\phi}^2\rangle_c}. \tag{45}$$

Here, for example, $\langle\tilde{\phi}^4\rangle_c$ is the connected part of vacuum expectation value of fourth power of the Fourier transform of the field at zero momentum. As we will show, in the weak coupling regime this method suffers from very noisy signals giving rise to large statistical errors. The errors are due to the large fluctuations of correlation functions in this regime as well as the subtraction of the disconnected pieces. However, in the strong coupling regime this method gives a relatively

good approximation for $\tilde{\Gamma}_c^{(4)}(0)$ and the statistical errors are reasonably small [14]. However, the higher-order vertex functions calculated with this approach can be very noisy even in the strong coupling regime, primarily due to subtractions of noisy disconnected pieces.

V. THE NUMERICAL RESULTS

In this section we present our results for the calculation of renormalized coupling λ_r in two dimensions. It includes the symmetric and broken symmetry sector in the weak coupling regime as well as the strong coupling regime. In the case of the weak coupling regime the results are compared with two-loop results and the direct calculation of λ_r using the standard MC method in Eq. (45). In the strong coupling regime we also compared the results of each method with the strong coupling expansion results. The details of the numerical simulation are included at the end of this article.

A. Case 1: The symmetric sector in the weak coupling regime (WCR)

1. The variation of the source method

Here we study the model in the symmetric sector where $\langle\phi\rangle=0$. As we will see, all methods presented in this paper require the calculation of renormalized mass $\hat{m}_r$, and the wave function renormalization constant Z. In general, the boson propagator extracted from the lattice has the form

$$\tilde{G}(\hat{k})=\frac{Z}{\hat{k}^2+\hat{m}_r^2(\hat{k}^2)}, \tag{46}$$

where $\hat{m}_r\equiv\hat{m}_r(\hat{m}_r^2)$ is the mass pole of the scalar particle, i.e., the renormalized mass. In particular at zero momentum

$$\tilde{G}(\hat{k}=0)=\frac{Z}{\hat{m}_r^2}, \tag{47}$$

where we make the standard approximation that $\hat{m}_r^2\approx\hat{m}_r^2(0)$. The renormalized mass $\hat{m}_r$ is then given as the reciprocal of $\hat{\xi}$, the lattice correlation length

$$\hat{\xi}^2=\frac{1}{\hat{m}_r^2}=\frac{1}{\tilde{G}(\hat{k})}\left.\frac{d\tilde{G}(\hat{k})}{d\hat{k}^2}\right|_{\hat{k}=0}. \tag{48}$$

Taking into account the translational invariance of the correlation functions, one can choose to approximate the momentum derivative in Eq. (48) by the variation of $\tilde{G}(\hat{k})$ across one lattice spacing and in one direction to obtain

$$\hat{\xi}^2=\frac{N}{2\pi}\left[\frac{\langle\gamma^2\rangle_c-\langle\alpha^2\rangle_c-\langle\beta^2\rangle_c}{\langle\alpha^2\rangle_c+\langle\beta^2\rangle_c}\right], \tag{49}$$

with

$$\alpha=\sum_{n=1}^{N}\sum_{m=1}^{N}\phi_{n,m}\cos\left[\frac{2\pi}{N}\left(n-\frac{N}{2}\right)\right],$$

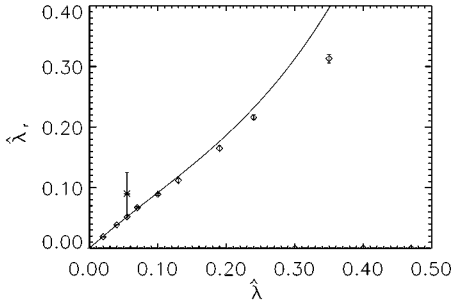

FIG. 3. Plot of $\hat{\lambda}_r$ versus $\hat{\lambda}$ in the symmetric sector using lattice perturbation theory (solid line) and Eq. (45) (stars) and the VSM (diamonds) with $\hat{m}^2=0.1$ and $N=20$.

$$\beta=\sum_{n=1}^{N}\sum_{m=1}^{N}\phi_{n,m}\sin\left\{\left[\frac{2\pi}{N}\left(n-\frac{N}{2}\right)\right]\right\},$$

$$\gamma=\sum_{n=1}^{N}\sum_{m=1}^{N}\phi_{n,m}, \tag{50}$$

where here n,m label the temporal and spatial coordinates for the field ϕ, respectively.

There are two different ways of calculating Z. One is to use Eq. (47) and the fact that $\tilde{G}(0)=N^2\langle\bar{\phi}^2\rangle$ to calculate Z. The second way of calculating Z comes from combining Eqs. (47) and (27) which gives

$$\left.\frac{d^2U(\bar{\phi})}{d\bar{\phi}^2}\right|_{\bar{\phi}=\langle\phi\rangle}=\frac{1}{\tilde{G}(0)}. \tag{51}$$

Thus $\tilde{G}(0)$ can be directly calculated from the fit and the calculation of Z follows as before. An accurate calculation of $\hat{m}_r$ is crucial for both methods. We found that in the weak coupling regime, the second method was more precise. We compared our results with the two-loop lattice perturbation theory calculations (LPT) of the renormalized parameters. This means that finite size effects may be present in our comparisons at some level. The comparison is shown in Fig. 3. The values for λ_r seem to be accurate even in the very weak coupling regime. In this regime the effective potential results are in good agreement with the lattice perturbation calculations. The MC results begin to deviate from the perturbative calculations as $\hat{\lambda}_r$ increases. This is expected since a loop expansion in $\lambda\phi^4$ theory is an expansion in $\hat{\lambda}_r$ and as this is increased the contribution from higher loops becomes more significant.

The VMS can be expensive in CPU time but the cost can be reduced to some extent. For a value of J it is possible to calculate $D^n(\phi)\equiv d\hat{\phi}_J^n/d^nJ=N^2\langle\tilde{\phi}^n\rangle_c$ during the calculation of ϕ_J, for each value of J. From these derivatives one can expand $\bar{\phi}_J$ around J and then use a curve fitting routine to calculate λ_r, as we did before. The statistical errors can become larger for the higher derivatives because of the subtraction of the disconnected pieces of $D^n(\phi)$. In Table I we have shown a comparison of our previous results for $\bar{\phi}_J$ and results obtained by expansion around three J values, namely,

TABLE I. Comparison of the calculations of $\bar{\phi}_J$ for different values of J's and perturbative calculations of $\bar{\phi}_J$ around $J=0.1$, $J=0.225$, and $J=0.425$ with $\hat{m}^2=0.1$, $\hat{\lambda}=0.055$, and $N=20$.

J	$\bar{\phi}_J$	Error	$[\bar{\phi}_J]_{\rm per}$	Error
0.050	0.4052	0.0032	0.409	0.0057
0.075	0.5841	0.0031	0.5880	0.0052
0.100	0.7648	0.0031	0.7648	0.0031
0.125	0.9253	0.0027	0.9320	0.0042
0.150	1.0840	0.0027	1.095	0.0048
0.175	1.2112	0.0027	1.218	0.0047
0.200	1.3399	0.0027	1.4510	0.0039
0.225	1.4505	0.0026	1.4505	0.0026
0.250	1.5590	0.0026	1.5646	0.0038
0.275	1.6659	0.0026	1.6680	0.0043
0.300	1.7620	0.0026	1.7720	0.0049
0.325	1.8564	0.0026	1.8706	0.0048
0.350	1.9411	0.0026	1.945	0.0038
0.375	2.0166	0.0026	2.0209	0.0033
0.400	2.0963	0.0026	2.0963	0.0026
0.425	2.1704	0.0026	2.1714	0.0029
0.450	2.2430	0.0026	2.2470	0.0029

$J=0.075,0.25,0.4$ for $\hat{m}^2=0.1$, $\hat{\lambda}=0.1$. We see that the calculated values of $\bar{\phi}$ are reasonably close to the previous results. However, the price for reduced computational time is a slight increase in uncertainties.

We have also calculated $\hat{\lambda}_r$ for $\hat{\lambda}=0.055$, $\hat{m}^2=0.1$ using Eq. (45) and the result is included in Fig. 3. The statistical errors are extremely large and it suggests that the calculation of the four-point vertex function in this region is impractical with this method.

2. The constraint effective potential method I

This method is the easiest to implement. We generated the Boltzmann ensemble of independent configurations. For every configuration we measured $\bar{\phi}=(1/N^2)\Sigma_i\phi_i$ and computed the histograms for the probability density $P(\bar{\phi})$ for several values of J. We also noticed that the ansatz of Eq. (39) only worked well for very small J in this region. We did a simultaneous fit to Eq. (36) of a few histograms corresponding to $J=0$ and small J's using a three-parameter ansatz for $\tilde{U}(\bar{\phi})$ of the form

$$\tilde{U}(\bar{\phi})=a_1\bar{\phi}^2+a_2\bar{\phi}^4+a_3\bar{\phi}^6. \tag{52}$$

Although there was no systematic discrepancy between the data and the fit, the statistical errors were very large. We unsuccessfully tried more histograms and higher powers of $\bar{\phi}$ in the fit. The statistical errors remained large and we concluded that even a reasonable estimate of renormalized parameters in this region was not feasible with this method.

3. The constraint effective potential method II

In this method Eqs. (A4) and (A8) can be used for calculations of $\hat{m}_r$ and $\hat{\lambda}_r$, respectively. All averages shown in these equations are to be taken with the constraint of $\bar{\phi}=0$. Although the statistical errors for each term are small, the overall error can be large. However, in the symmetric case in the weak coupling regime most of the terms either vanish at $\bar{\phi}=0$ or are small enough to be neglected. For example, for $\hat{m}_r$ only three terms need to be considered. But the computation of $\hat{\lambda}_r$ suffers from larger cumulative errors.

TABLE II. Comparison of the calculations of $\hat{\lambda}_r$ using the VSM and the CEP II in the symmetric sector and weak coupling regime. $\hat{\lambda}_r^{\rm cons}$ denotes the renormalized coupling calculated by CEP II. Here $\hat{m}^2=0.1$ and $N=20$.

$\hat{\lambda}$	$\hat{\lambda}_r^s$	Error	$\hat{\lambda}_r^{\rm cons}$	Error
0.02	0.0191	0.0003	0.018	0.0007
0.04	0.0386	0.0003	0.0363	0.0008
0.055	0.0518	0.0008	0.0510	0.0017
0.07	0.0670	0.0009	0.0657	0.0019
0.1	0.0891	0.0008	0.092	0.0016
0.13	0.112	0.0013	0.121	0.004
0.19	0.165	0.002	0.175	0.0061
0.24	0.216	0.0023	0.22	0.007
0.35	0.313	0.0035	0.321	0.018

The field wave function renormalization constant Z can be calculated in two different ways. One can use Eq. (47) and relation $\tilde{G}(0)=N^2\langle\tilde{\phi}^2\rangle$, as in the previous case, or one can use Eq. (47) and Eq. (51) where $[d^2U(\bar{\phi})/d\bar{\phi}^2]|_{\bar{\phi}=\langle\phi\rangle}$ can be found from Eq. (A4).

The results are compared with the VSM results and are shown in Table II. We also compared the calculation of renormalized mass using Eq. (49) with the CEP II calculations in Table III. The comparison indicates that in this sector the CEP II method can provide an accurate calculation of the renormalized vertex functions.

B. Case 2: The broken symmetry sector

In this section we consider the calculation of the renormalized mass and renormalized coupling in the broken sec-

TABLE III. Comparison of the calculations of $\hat{m}_r^2$ using the VSM and the CEP II in the symmetric sector and weak coupling regime. $\hat{\lambda}_r^{\rm cons}$ denotes the renormalized mass calculated by CEP II. Here $\hat{m}^2=0.1$ and $N=20$.

$\hat{\lambda}$	$\hat{m}_r$	Error	$\hat{m}_r^{\rm cons}$	Error
0.02	0.324	0.001	0.323	0.007
0.04	0.334	0.002	0.330	0.007
0.055	0.340	0.0008	0.332	0.008
0.07	0.343	0.0014	0.339	0.006
0.1	0.345	0.0023	0.347	0.008
0.13	0.350	0.0023	0.357	0.009
0.19	0.375	0.0025	0.372	0.009
0.24	0.398	0.003	0.384	0.010
0.3	0.408	0.003	0.399	0.009
0.35	0.421	0.0035	0.410	0.010
0.40	0.433	0.004	0.428	0.010

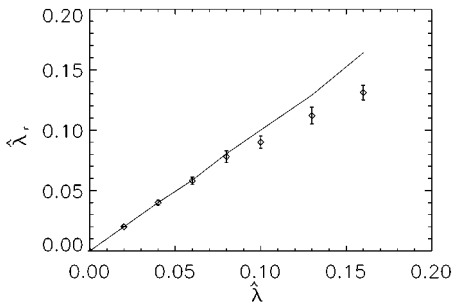

FIG. 4. The plot of $\hat{\lambda}_r$ versus $\hat{\lambda}$ in the broken symmetry sector $\hat{\lambda}$ using lattice perturbation theory (solid line) and VSM (diamonds) with $\hat{m}^2=-0.1$ and $N=20$.

tor, $\langle\phi\rangle\neq 0$, in the weak coupling regime. The VSM procedure is exactly the same as for the symmetric sector. For fixed $\hat{m}^2=-0.1$ and $0<\hat{\lambda}\leqslant 0.17$ we calculated $\hat{m}_r$ and $\hat{\lambda}_r$ for different values of $\hat{\lambda}$. The error on $\widetilde{G}(0)$ is larger than the symmetric case due to the subtraction of the disconnected pieces. Thus we used Eq. (51) to calculate $\widetilde{G}(0)$ and subsequently extracted Z as previously discussed.

In order to calculate the renormalized quantities using lattice perturbation theory we followed the standard approach to treating the broken sector. That is, in the bare Lagrangian we shifted the field by its vacuum expectation value (ν), which can be easily calculated using MC methods, such that

$$\chi(x)\equiv\phi(x)-\nu. \tag{53}$$

After this translation the mean value of the shifted field, $\langle\chi\rangle$, vanishes and the perturbative calculation proceeds in the standard manner, keeping in mind that a nonsymmetric χ^3 interaction has been generated. In lattice perturbation theory one then needs to also consider vertex functions with a three-point interaction. Note that ν can be different from the classical value of the vacuum, $\nu_{\rm cl}=\sqrt{-6\hat{m}^2/\hat{\lambda}}$. As an example, for $\hat{m}^2=-0.1$ and $\hat{\lambda}=0.1$ we find $\nu=2.181\pm 0.002$, which is to be compared with $\nu_{\rm cl}=2.449$.

The comparison between the two-loop results and the results from the VSM method is shown in Fig. 4. In applying the CEP II method to the broken symmetry sector, evaluation of all the terms in Eq. (A8) is necessary. This renders this method impractical. As one might expect from the symmetric sector results the calculation of the renormalized parameters using CEP I also suffers from large noise difficulties and the signal could not be recovered.

C. Case 3: Strong coupling regime

In a weak coupling expansion the interactive term is pulled out of the path integral representation of the partition function as a functional operator. That is

$$Z[\hat{J}]=\exp\left[\frac{\hat{\lambda}}{4!}\sum_n\ \frac{\delta^4}{\delta\hat{J}_n^4}\right]\int[d\phi]\exp\left[-\sum_{n,\mu}\ \frac{1}{2}(\phi_n-\phi_{n,\mu})^2+\frac{1}{2}\hat{m}^2\phi_n^2+\hat{J}_n\phi_n\right]. \tag{54}$$

The remaining functional is Gaussian and can be done exactly. The partition function can then be written in terms of a power series of $\hat{\lambda}$ and the standard perturbation theory follows.

The strong coupling expansion was first proposed by the authors of Ref. [15]. For this expansion, unlike the weak coupling expansion, the kinetic and the mass terms are pulled out of the path integral as a functional operator. That is

$$Z[\hat{J}]=\exp\left[\sum_{m,n}\ \frac{\delta}{\delta\hat{J}_n}\,G^{-1}(n,m)\,\frac{\delta}{\delta\hat{J}_m}\right]Z_0[\hat{J}], \tag{55}$$

where

$$Z_0[\hat{J}]=\int[d\phi]\exp\left[\sum_n\ \frac{\hat{\lambda}}{4!}\,\phi_n^4+\hat{J}_n\phi_n\right]. \tag{56}$$

The remaining functional integral is not Gaussian but can be evaluated as a product of ordinary functions on the lattice,

$$Z_0[\hat{J}]=\mathcal{N}\prod_n\ \frac{F(x)}{F(0)}, \tag{57}$$

where

$$F(x)\equiv\int dz e^{-[(\hat{\lambda}/4!)z^4+xz]} \tag{58}$$

and $\mathcal{N}$ is a constant. The function $F(x)$ is a transcendental function and can be expanded as a power series in x,

$$F(x)=\frac{1}{\sqrt{(2)}}\sum_{n=0}^{\infty}\ \frac{2^n x^{2n}}{(2n)!}\Gamma\left(\frac{n}{2}+\frac{1}{4}\right). \tag{59}$$

Using this series expansion one can easily expand both terms in the right-hand side of Eq. (55) to obtain a power series expansion for $Z[J]$ which assumes the general form

$$Z[\hat{J}]=\mathcal{N}'\left[1+\sum_{k=1}^{\infty}\ \hat{\lambda}^{-k/2}A_k[\hat{J}]\right], \tag{60}$$

where $A_k[\hat{J}]$ are integrals over the source function J. Thus the strong coupling expansion is an expansion in powers of $\hat{\lambda}^{-k/2}$. Bender *et al.* [15,16] obtained a series expansion for a quantity that we denote here by g_R, where $g_R\equiv\hat{\lambda}_r/\hat{m}_r^{4-d}$. This expansion has the form

$$g_R=y^{-d/2}\sum_{l=0}^{L}\sum_{n=0}^{N}\ a_{nl}x^n y^l, \tag{61}$$

where

$$x=y^{-d/2}\frac{\hat{m}_r^2}{\hat{\lambda}_r}\quad\text{and}\quad y=\hat{\xi}^2=\frac{1}{\hat{m}_r}. \tag{62}$$

For fixed x one has

$$g_R = y^{-d/2} \sum_{l=0}^{L} a_l^{(N)}(x) y^l, \tag{63}$$

where

$$a_l^{(N)}(x) = \sum_{n=0}^{N} a_{ln} x^n. \tag{64}$$

This series does not converge for large correlation lengths. Thus the authors of Ref. [16] proposed a scheme to extrapolate the expression for $\hat{\lambda}_r$ to large y assuming that $\hat{\lambda}_r$ remains finite in the limit $y \to 0$.

Raising Eq. (61) to the power of $2L/d$ and expanding to order L we find

$$g_R^{2L/d} = y^{-L} \left(\sum_{l=0}^{L} a_l^{(N)}(x) y^l \right)^{2L/d} \equiv y^{-L} \sum_{l=0}^{L} b_l^{(N)}(x) y^l. \tag{65}$$

We then find

$$g_R = y^{-d/2} \left(\sum_{l=0}^{L} b_l(x) y^l \right)^{(d/2L)}, \tag{66}$$

which is equivalent to Eq. (61) for small y and approaches $[b_L^N(x)]^{d/2l}$ in the limit $y \to \infty$. In this manner the authors of Ref. [17] obtained an analytical series for Eq. (66). Since the interesting physics lies in a regime where the correlation length is large, we performed our calculation in this regime. Thus the above extrapolation scheme was necessary.

We chose a moderate correlation length $\xi = 3.6$ by an appropriate tuning of the bare parameters. This can be done by fixing $\hat{\lambda}$ and choosing $\hat{m}$ to be in the symmetric region. As one decreases $\hat{m}$, one gets closer to the critical line and the correlation length increases. Using this, one can reach the required correlation length.

To apply VSM we followed the same procedure as before. For six different $\hat{\lambda}$'s and fixed correlation length $\xi = 3.6(\mp 4\%)$, we calculated the values of $\overline{\phi}_J$ for different values of J. The curve fitting procedure was carried out in the same way as for the previous cases. We noticed that in this regime the inclusion of larger ϕ_J's can change the behavior of the fit at small ϕ_J, the region which is of most interest to us. The problem arises due to the curve fitting procedure. In the weak coupling regime, the data points close to $\overline{\phi} = 0$ have much larger weighting than the one far away from this point. Thus calculating the derivatives of $U(\overline{\phi})$ at $\overline{\phi} = 0$ seems to be reliable. However, in the strong coupling regime, the data points that are far away from $\overline{\phi} = 0$ have much higher weighting and even a small fluctuation might affect the calculated $J(\overline{\phi})$ considerably.

We improved the results by imposing the condition in Eq. (51), that is to fixing the coefficient $a_1 = 1/\hat{G}(0)$ where a_1 is defined in Eq. (52) and $\tilde{G}(0) = N^2 \langle \tilde{\phi}^2 \rangle$. This improved the results and the inclusion of larger ϕ_J's did not affect the results significantly (up to 3%).

Next we calculated the renormalized parameters using CEP I. Unlike the previous cases the errors in the results were reasonable. For the extraction of renormalized parameters we only used two histograms corresponding to $J = 0$ and $J = 0.005$. In the weak coupling regime where the mass term is dominant, one needs to sample the higher values of $\overline{\phi}$ in order to improve the calculation of $\hat{\lambda}_r$. Thus in the strong coupling regime there might not be a need for additional histograms. From the VSM results one might expect that sampling very high $\overline{\phi}$ might have a similar problem. This was confirmed from our data for this particular case.

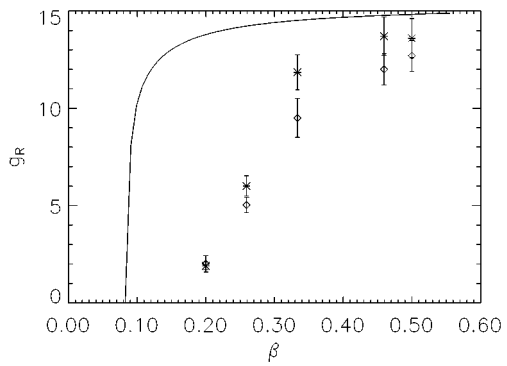

FIG. 5. The plot of $g_R = \hat{\lambda}_r / \hat{m}_r^2$ versus $\beta \equiv \hat{\lambda}/(\hat{\lambda} + 100)$ with strong coupling expansion results (solid line), using Eq. (45) (stars) and the VSM results (diamonds) with $\hat{m}_r^2 = 0.078(\pm 4\%)$ and $N = 20$.

We also calculated the renormalized coupling using Eq. (45). Unlike the weak coupling regime, uncertainties in the results in this region were reasonable. All the results in the strong coupling regime are shown in Figs. 5 and 6. In these figures we plot $g_R = \hat{\lambda}_r / \hat{m}_r^2$ as a function of β, where we have defined for convenience $\beta \equiv \hat{\lambda}/(\hat{\lambda} + 100)$. As $\hat{\lambda} \to \infty$ we have $\beta \to 1$, which is the strong coupling limit. They were also compared with the strong coupling expansion results. They all seem to be in agreement with each other within errors. This indicates that as the coupling increases the MC results approach the strong coupling expansion results. In the strong coupling expansion, the value of g_R with $\xi = 3.6$ approaches 14.88 ∓ 0.04 as $\beta \to 1$. This value depends on the correlation length. In order to apply the CEP II method, there are numerous terms in Eq. (A8) which have to be evaluated

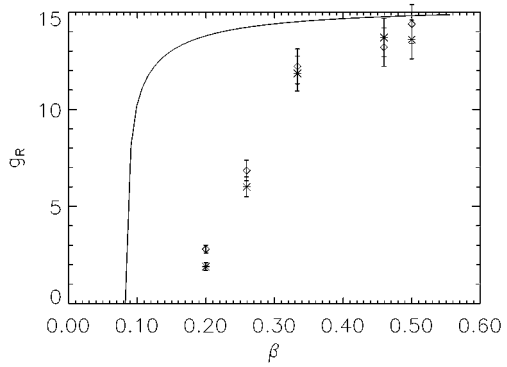

FIG. 6. The plot of $g_R = \hat{\lambda}_r / \hat{m}_r^2$ versus $\beta \equiv \hat{\lambda}/(\hat{\lambda} + 100)$ with strong coupling expansion results (solid line), using Eq. (45) (stars) and the CP II method results (diamonds) with $\hat{m}_r^2 = 0.078(\pm 4\%)$ and $N = 20$.

and consequently the accumulated errors can be very large. However, we found that as before the renormalized mass can be calculated accurately.

D. Details of the simulations

In our MC calculation we chose the hybrid MC algorithm. In a run we have taken a number of decorrelation MC iterations between two measurements. All the calculations were done on a 20^2 lattice and the rate of acceptance was kept between 40% and 60%. In all cases (except the broken sector) the calculations of renormalized mass and $\tilde{G}(0)$ (where it was needed) and the direct calculation of $\tilde{\Gamma}_c^{(4)}(0)$ were done using 6800 uncorrelated samples with 50 000 thermalization configurations. In the broken sector we used 11 000 uncorrelated samples with the same thermalization configurations. The reason for the increase was to obtain better statistics, since the measured quantities have larger errors due to the non-vanishing disconnected pieces. In applying the VSM to the symmetric case (and in the weak coupling regime), we calculated $\overline{\phi}$ with $0.025 \leqslant J \leqslant 0.425$. We noticed that the necessary number of decorrelation iterations in the presence of nonzero J was smaller than for the $J=0$ case. The calculations were carried out using 2500 decorrelated configurations. We took the number of thermalization configurations to be 10 000. In the broken symmetry sector we increased the number of uncorrelated configurations to 3200. In the strong coupling regime only the range of the values for J was different (as mentioned in the preceding section). For CEP II we used 5000 uncorrelated configurations with 50 000 thermalization iterations. In construction of the probability distribution histograms, we used 750 000 configurations. The curve fits were done using a standard χ^2 fitting algorithm where the uncertainties on the parameters were obtained from the diagonal of the covariant matrix. For the strong coupling results we also estimated the systematic error due to the fact that $\hat{\zeta}$ was fixed to be approximately 4% by varying the fixed value within reasonable limits.

VI. CONCLUSIONS

We have studied the calculation of the effective potential for $\lambda\phi^4_{1+1}$ theory using three different methods: the variation of source method and two constraint effective potential methods (CEP I and CEP II). Using our method, referred to as CEP II, we showed how to calculate the vertex function using the correlation functions in the presence of a constraint. We calculated the effective potential in the symmetric and the broken sector in the weak coupling regime as well as in the symmetric sector in the strong coupling regime. The renormalized quantities $\hat{\lambda}_r$ and $\hat{m}_r$ were then obtained from the effective potential for each case. In the weak coupling regime we compared our results with lattice perturbation theory. We found that in the symmetric case both VSM and CEP II can give accurate results, whereas the CEP I method and the direct Monte Carlo calculation of the (two- and four-point) vertex functions failed to do so. We also found that in the broken symmetry sector VSM is the most practical and accurate of these methods. We also studied the model in the strong coupling regime and the results were compared with the strong coupling expansion results. In this regime we found that CEP I, VSM, and the results from the direct Monte Carlo calculation of the vertex functions were consistent with each other and with the strong coupling expansion results. In summary then, we have shown that Monte Carlo effective potential methods can be accurate and reliable tools for calculating physical quantities for scalar field theories, but that one should use the method of evaluating the effective potential and its derivatives which is best suited to the regime of interest.

APPENDIX

The differential equations relating the constraint effective potential and the classical potential follow.

For the first derivative we have

$$\frac{dU(\overline{\phi})}{d\overline{\phi}} = \left\langle \frac{dV(\phi)}{d\phi} \right\rangle_{\overline{\phi}}, \tag{A1}$$

which for $\lambda\phi^4$ theory becomes

$$\frac{dU(\overline{\phi})}{d\overline{\phi}} = m^2\overline{\phi} + \frac{\lambda}{6}\langle\phi^3\rangle. \tag{A2}$$

The second derivative is given by

$$\frac{d^2U(\overline{\phi})}{d\overline{\phi}^2} = \left\langle \frac{d^2V(\phi_1)}{d\phi_1^2} \right\rangle_{\overline{\phi}} - \sum_{i=1}^{N^d} \left\langle \frac{dV(\phi_1)}{d\phi_1}\frac{dV(\phi_i)}{d\phi_i} \right\rangle_{\overline{\phi}} + N^d \left(\left\langle \frac{dV(\phi_1)}{d\phi} \right\rangle_{\overline{\phi}} \right)^2, \tag{A3}$$

which for $\lambda\phi^4$ theory becomes

$$\begin{aligned}\frac{d^2U(\overline{\phi})}{d^2\overline{\phi}} &= m^2 + \frac{\lambda}{2}\langle\phi^2\rangle \\ &\quad + N^d\left[\frac{\lambda^2}{36}\langle\phi^3\rangle^2 + \frac{\lambda m^2}{3}\,\overline{\phi}\langle\phi^3\rangle + m^4\overline{\phi}^2\right] \\ &\quad - N^d\left[m^4\langle\phi\tilde{\phi}\rangle + \frac{\lambda m^2}{6}\langle\phi^3\tilde{\phi}\rangle + \frac{\lambda^2}{36}\langle\phi^3\tilde{\phi}^3\rangle \right. \\ &\quad \left. + \frac{\lambda m^2}{6}\langle\phi\tilde{\phi}^3\rangle\right].\end{aligned} \tag{A4}$$

The third derivative gives

$$\begin{aligned}\frac{d^3U(\overline{\phi})}{d\overline{\phi}^3} &= N^d\frac{d^2U(\overline{\phi})}{d\overline{\phi}^2}\frac{dU(\overline{\phi})}{d\overline{\phi}} + 2N^d\left(\frac{dU(\overline{\phi})}{d\overline{\phi}}\right)^2 \\ &\quad - N^{2d}\left(\frac{dU(\overline{\phi})}{d\overline{\phi}}\right)^3 + \left\langle\frac{d^3V(\phi_1)}{d\phi_1^3}\right\rangle_{\overline{\phi}} + \cdots,\end{aligned} \tag{A5}$$

which for $\lambda\phi^4$ theory becomes

$$\frac{d^3U(\bar{\phi})}{d\bar{\phi}^3}=\hat{m}^2\frac{\hat{\lambda}}{6}\langle\phi^3\rangle-N^d\frac{\hat{\lambda}}{6}\langle\phi^2\tilde{\phi}^3\rangle-N^d\hat{\lambda}\langle\phi^2\tilde{\phi}\rangle$$
$$+[O(\hat{\lambda}^2)\ \text{terms}]+[O(\hat{m}^2)\ \text{terms}]$$
$$+[\text{terms that vanish at }\bar{\phi}=0]+\cdots . \tag{A6}$$

Finally, for the fourth derivative we obtain

$$\frac{d^4U(\bar{\phi})}{d\bar{\phi}^4}=N^d\left\langle\frac{d^2U(\bar{\phi})}{d\bar{\phi}^2}\right\rangle^2-4N^{2d}\frac{d^2U(\bar{\phi})}{d\bar{\phi}^2}\left\langle\frac{dU(\bar{\phi})}{d\bar{\phi}}\right\rangle^2$$
$$+\left\langle\frac{d^4V(\phi_1)}{d\phi_1}\right\rangle_{\bar{\phi}}+\cdots , \tag{A7}$$

which for $\lambda\phi^4$ theory gives

$$\frac{d^4U(\bar{\phi})}{d\bar{\phi}^4}=\hat{\lambda}-\lambda\hat{m}^2-N^d\lambda\hat{m}^2\langle\tilde{\phi}^2\rangle-N^d\hat{\lambda}\hat{m}^2\langle\phi^2\rangle$$
$$+[O(\lambda^2)\ \text{terms}]+[O(\hat{m}^4)\ \text{terms}]$$
$$+[\text{terms that vanish at }\bar{\phi}=0]. \tag{A8}$$

[1] S. Coleman and E. Weinberg, Phys. Rev. D **7**, 1888 (1973).
[2] R. Jakiw, Phys. Rev. D **9**, 1686 (1974).
[3] S. Coleman, R. Jakiw, and H. D. Politzer, Phys. Rev. D **10**, 2491 (1974).
[4] K. Symanzik, Commun. Math. Phys. **16**, 48 (1970).
[5] Y. Fujimoto, L. O'Raifeartaigh, and G. Parravicini, Nucl. Phys. B **122**, 268 (1984).
[6] D. J. E. Callaway and D. J. Maloof, Phys. Rev. D **27**, 406 (1983).
[7] K. Huang, E. Manousakis, and J. Polonyi, Phys. Rev. D **35**, 3187 (1987).
[8] R. Fukuta and E. Kyrikopoulos, Nucl. Phys. B **85**, 354 (1975).
[9] I. Montvay and I. Munster, *Quantum Fields on the Lattice* (Cambridge University Press, Cambridge, England, 1994).
[10] K. G. Wilson and J. Kogut, Phys. Rep., Phys. Lett. **12C**, 76 (1974).
[11] L. O'Raifeartaigh, A. Wipf, and H. Yoneyama, Nucl. Phys. B **271**, 653 (1986).
[12] G. J. Lasino, in *Scaling and Self-similarity in Physics*, edited by J. Frohlich (Birkhauser, Basel, 1983).
[13] M. M. Tsypin, Phys. Rev. Lett. **73**, 2015 (1994).
[14] F. Cooper, B. Freedman, and D. Preston, Nucl. Phys. B: Field Theory Stat. Syst. **210**, [FS6] 210 (1982).
[15] C. M. Bender, F. Cooper, G. S. Guralnik, and D. Sharp, Phys. Rev. D **19**, 1865 (1979).
[16] C. M. Bender, F. Cooper, G. S. Guralnik, R. Roskies, and D. Sharp, Phys. Rev. D **23**, 2976 (1981).
[17] G. A. Baker, L. P. Benofy, F. Cooper, and D. Preston, Nucl. Phys. B: Field Theory Stat. Syst. **210**, [FS6] (1982).